Realizing one-dimensional topological superfluids with ultracold atomic gases



2013 J. Phys. B: At. Mol. Opt. Phys. 46 134005

(http://iopscience.iop.org/0953-4075/46/13/134005)

J. Phys. B: At. Mol. Opt. Phys. **46** (2013) 134005 (12pp) doi:10.1088/0953-4075/46/13/134005

# Realizing one-dimensional topological superfluids with ultracold atomic gases

**Sylvain Nascimbène**

Laboratoire Kastler Brossel, CNRS, UPMC, École Normale Supérieure, 24 rue Lhomond, F-75005 Paris, France

E-mail: sylvain.nascimbene@lkb.ens.fr

Received 1 October 2012, in final form 4 February 2013
Published 24 June 2013
Online at stacks.iop.org/JPhysB/46/134005

**Abstract**
We propose an experimental implementation of a topological superfluid with ultracold fermionic atoms. An optical superlattice is used to juxtapose a 1D gas of fermionic atoms and a 2D conventional superfluid of condensed Feshbach molecules. The latter acts as a Cooper pair reservoir and effectively induces a superfluid gap in the 1D system. Combined with a spin-dependent optical lattice along the 1D tube and laser-induced atom tunnelling, we obtain a topological superfluid phase. In the regime of weak couplings to the molecular field and for a uniform gas, the atomic system is equivalent to Kitaev's model of a p-wave superfluid. Using a numerical calculation, we show that the topological superfluidity is robust beyond the perturbative limit and in the presence of a harmonic trap. Finally, we describe how to investigate some physical properties of the Majorana fermions located at the topological superfluid boundaries. In particular, we discuss how to prepare and detect a given Majorana edge state.

(Some figures may appear in colour only in the online journal)

## 1. Introduction

Since the discovery of topological insulators [1, 2], the search for exotic states of matter with non-trivial topology such as a topological superconductor has generated strong interest. A non-trivial topological phase is characterized by a gap in the bulk elementary excitations and a non-local topological order associated with gapless states at the system edges, defects or vortex cores [3–8]. In topological superconductors, these edge states can be described as Majorana fermions, which are quasi-particles equal to their own antiparticles and obeying non-Abelian quantum statistics [9].

The simplest model of a topological superfluid was introduced by Kitaev in 2001 [6]. It consists of a 1D lattice system of spinless fermions with a p-wave superfluid gap, described by the Hamiltonian

$$\hat{H}_{\text{Kitaev}} = \sum_i -\mu\left(\hat{c}_i^\dagger \hat{c}_i - \frac{1}{2}\right) - J(\hat{c}_i^\dagger \hat{c}_{i+1} + \text{h.c.}) + \Delta(\hat{c}_i^\dagger \hat{c}_{i+1}^\dagger + \text{h.c.}), \quad (1)$$

where $\hat{c}_i^\dagger$ creates a fermion into the lattice site $i$, and $\mu$, $J$, $\Delta$ represent the chemical potential, the tunnelling amplitude and the superfluid gap, respectively. However this 'toy model' cannot be directly realized with solid-state systems. Subsequently, several proposals described how to create topological superconductors in solid-state heterostructures combining the superconducting proximity effect with a topological insulator or a semiconductor with the strong spin–orbit coupling [10–14]. These proposals led to the first observations of boundary quasiparticles behaving as Majorana fermions in 2012 [15–18].

Ultracold atomic gases constitute an alternative system for realizing a topological superfluid [19–24]. The extreme purity of these gases could allow one to realize model systems in a clean and controlled manner [25]. As described in [26, 27], the study of atomic Majorana fermions would also benefit from measurement techniques specific to atomic physics. While inducing topological superfluidity using resonant p-wave interactions cannot be achieved due to large inelastic loss rates [19, 28, 29], one expects that, in a quasi-2D Fermi gas, combining s-wave interactions with the Rashba-type spin–orbit coupling may lead to the formation of a $p_x + ip_y$ superfluid, which has a non-trivial topology [30–35]. Alternatively, by analogy with proximity-induced superconductivity [36], superfluidity could be induced by the

 

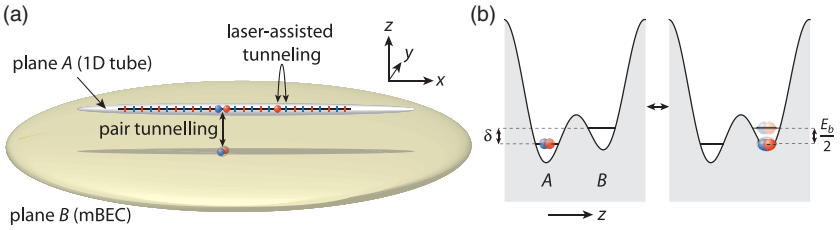


**Figure 1.** (a) General scheme of the setup, consisting of quasi-1D gases of fermionic atoms coupled to a 2D gas of condensed molecules. The tunnelling of atom pairs into the 1D tubes acts as a superfluid gap applied externally. A spin-dependent optical lattice is applied along the tube, leading to an effective lattice with spin ↑ (↓) particles localized in the even (odd) sites. Atom tunnelling inside the tube is driven by Raman lasers, leading to the realization of Kitaev's model of a p-wave superfluid. (b) Scheme of the atom pair tunnelling from $A$ to $B$, resonant for $E_b = 2\,\delta$.

coherent coupling to a molecular Bose–Einstein condensate (BEC) rather than by interatomic interactions [23].

In this paper, we propose an experimental implementation of a topological superfluid with ultracold Fermi gases based on proximity-induced superfluidity [23]. We use a superlattice potential to juxtapose a quasi-2D gas of condensed Feshbach molecules and a set of 1D tubes. The coupling of atom pairs between both systems effectively creates an s-wave superfluid gap in the 1D tubes. In addition, the atoms in the 1D tubes are held in a spin-dependent optical lattice, in which atom tunnelling is induced by the appropriate laser transitions. The scheme makes use of several ingredients—such as quasi-2D Fermi gases [37–40], spin-dependent potentials [41–45] or laser-induced atom tunnelling [46, 47]—that were already developed in the cold atom community. We show that this setup leads to the realization of a topological superfluid, which is equivalent to Kitaev's model in the perturbative regime of weak coupling to the molecular field. For stronger couplings, we obtain a robust topological superfluid with a large bulk gap value, both for homogeneous and harmonically trapped systems. Finally, we describe some measurable physical properties of a trapped atomic gas in this lattice geometry, which should exhibit a topological superfluid phase with Majorana fermions at its boundaries. In particular, we discuss how to prepare and detect a given Majorana edge state.

## 2. Proximity-induced superfluidity

Before describing the implementation of Kitaev's model, we first discuss the realization of proximity-induced s-wave superfluidity in a two-dimensional geometry. We consider a pair of quasi-2D atomic systems (planes $A$ and $B$) that can be created using a double-well potential along $z$ (see figure 1(b)). Plane $B$ is filled with a two-component Fermi gas, with effective spins labelled $|\uparrow\rangle$ and $|\downarrow\rangle$. We assume that a Feshbach resonance is used to create weakly bound Feshbach molecules [39, 40], and that the gas is cooled sufficiently to form a nearly pure molecular Bose–Einstein condensate (mBEC). When coupled to plane $A$ as described below, this system will act as a reservoir of Cooper pairs and effectively induce a superfluid gap in $A$ [23].

### *2.1. Effective Hamiltonian of a gas coupled to a molecular BEC*

The reservoir of condensed molecules in plane $B$ is described by a coherent state with a mean number of molecules $N$. The 2D wavefunction of a single molecule is written as

$$\phi_{\rm mol}(\boldsymbol{\rho}_\uparrow, \boldsymbol{\rho}_\downarrow) = \frac{1}{L}\phi_{\rm rel}(\boldsymbol{\rho}_\uparrow - \boldsymbol{\rho}_\downarrow), \tag{2}$$

where $L$ is the size of the quantification box along $x$ and $y$ and

$$\phi_{\rm rel}(\boldsymbol{\rho}) = \frac{1}{\sqrt{\pi}a}K_0(\rho/a) \tag{3}$$

is the 2D molecular wavefunction for the relative motion [48]. Here, $a$ denotes the 2D scattering length, $\boldsymbol{\rho}$ is the vector position in 2D and $K_0$ is a modified Bessel function of the second kind. The molecular binding energy will be written as $E_b = \hbar^2/ma^2$.

The coupling from the reservoir to plane $A$ occurs via atom tunnelling through the $A-$B barrier, described by a Hamiltonian

$$\hat{H}_z = -J_z \int {\rm d}\boldsymbol{\rho}\ (\hat{\psi}^\dagger_{A,\uparrow}(\boldsymbol{\rho})\hat{\psi}_{B,\uparrow}(\boldsymbol{\rho}) + \hat{\psi}^\dagger_{A,\downarrow}(\boldsymbol{\rho})\hat{\psi}_{B,\downarrow}(\boldsymbol{\rho})) + {\rm h.c.}, \tag{4}$$

where $J_z$ is the single-atom tunnelling amplitude and $\hat{\psi}^\dagger_{X,\sigma}(\boldsymbol{\rho})$ denotes the creation operator of a particle of spin $\sigma$ in plane $X$.

We expect that tunnelling of atoms towards plane $A$ leads to the dissociation of molecules, leading to pairs of atoms of opposite spin in both planes $A$ and $B$[1]. These dissociated atom pairs can be described by an effective Hamiltonian using a semi-classical approximation, which consists in replacing the mBEC by a classical field. By analogy with the Glauber unitary transform for coherent states of the electromagnetic field [49], we define the effective Hamiltonian as

$$\hat{H}_{z,\rm eff} = \hat{D}^\dagger_{\rm mBEC}\hat{H}_z\hat{D}_{\rm mBEC}, \tag{5}$$

where

$$\hat{D}_{\rm mBEC} = {\rm e}^{-\sqrt{\rm N}/2}\exp(\sqrt{\rm N}(\hat{\psi}^\dagger_{\rm mol} - \hat{\psi}_{\rm mol})) \tag{6}$$

is the displacement operator that brings the mBEC to the vacuum state and

$$\psi^\dagger_{\rm mol} = \int {\rm d}\boldsymbol{\rho}_\uparrow {\rm d}\boldsymbol{\rho}_\downarrow\ \phi_{\rm mol}(\boldsymbol{\rho}_\uparrow, \boldsymbol{\rho}_\downarrow)\hat{\psi}^\dagger_{B,\uparrow}(\boldsymbol{\rho}_\uparrow)\hat{\psi}^\dagger_{B,\downarrow}(\boldsymbol{\rho}_\downarrow) \tag{7}$$

creates a molecule in plane $B$.

[1] Note that the tunnelling of bound molecules to plane $A$ is prevented by the spin-dependent optical lattice described in the following.

The effective Hamiltonian can be calculated explicitly as a series in $k_F a$, where $k_F = 2\sqrt{\pi}\sqrt{N}/L$ is the Fermi momentum in plane $B$ (see appendix A). As we are interested in the molecular regime $k_F a \ll 1$, we only keep for simplicity the first term in $k_F a$, leading to a Hamiltonian $\hat{H}_{z,\mathrm{eff}} = \hat{H}_z + \hat{H}_{\mathrm{pairs}}$, where the additional term

$$\hat{H}_{\mathrm{pairs}} = -J_z \frac{k_F}{2\sqrt{\pi}} \int \mathrm{d}\boldsymbol{\rho}_\uparrow \mathrm{d}\boldsymbol{\rho}_\downarrow \, \phi_{\mathrm{rel}}(\boldsymbol{\rho}_\uparrow - \boldsymbol{\rho}_\downarrow) \times (\hat{\psi}^\dagger_{B,\uparrow}(\boldsymbol{\rho}_\uparrow)\hat{\psi}^\dagger_{A,\downarrow}(\boldsymbol{\rho}_\downarrow) + \hat{\psi}^\dagger_{A,\uparrow}(\boldsymbol{\rho}_\uparrow)\hat{\psi}^\dagger_{B,\downarrow}(\boldsymbol{\rho}_\downarrow) + \mathrm{h.c.}) \tag{8}$$

describes the creation (or annihilation) of pairs of particles dissociated from the mBEC. We show in appendix A that the neglected terms of the series have minor effects for the parameters used in the following.

An additional energy offset $\delta$ is introduced in plane $B$ in order to match the resonance condition $2\delta = E_b$ (see figure 1(b)), described by the Hamiltonian

$$\hat{H}_\delta = \delta \int \mathrm{d}\boldsymbol{\rho} \, (\hat{\psi}^\dagger_{A,\uparrow}(\boldsymbol{\rho})\hat{\psi}_{A,\uparrow}(\boldsymbol{\rho}) + \hat{\psi}^\dagger_{A,\downarrow}(\boldsymbol{\rho})\hat{\psi}_{A,\downarrow}(\boldsymbol{\rho})). \tag{9}$$

The total effective Hamiltonian is then given by the expression

$$\hat{H}_\Delta = \hat{H}_{\mathrm{kin}} + \hat{H}_{\mathrm{pot}} + \hat{H}_z + \hat{H}_{\mathrm{pairs}} + \hat{H}_\delta, \tag{10}$$

where $\hat{H}_{\mathrm{kin}}$ and $\hat{H}_{\mathrm{pot}}$, respectively, denote the 2D kinetic energy operator and the potential energy due to additional potentials applied externally.

### *2.2. Superfluid gap in the weak coupling regime*

A simple picture of the system can be obtained in the limit $J_z \ll \delta$ where at low energy all non-condensed atoms are located in plane $A$ and plane $B$ is only virtually populated by single atoms. In second-order perturbation theory, the system can be described by an effective Hamiltonian restricted to plane $A$ [50],

$$\hat{H}^{(2)}_\Delta = -\hat{P}_A \frac{(\hat{H}_{\mathrm{kin}} + \hat{H}_{\mathrm{pot}} + \hat{H}_z + \hat{H}_{\mathrm{pairs}})^2}{\delta} \hat{P}_A, \tag{11}$$

where $\hat{P}_A$ projects on the Hilbert space of wavefunctions localized in plane $A$. A straightforward calculation leads to

$$\hat{H}^{(2)}_\Delta = \hat{H}_{\mathrm{kin}} + \hat{H}_{\mathrm{pot}} + \int \mathrm{d}\boldsymbol{\rho}_\uparrow \mathrm{d}\boldsymbol{\rho}_\downarrow \, \Delta(\boldsymbol{\rho}_\uparrow - \boldsymbol{\rho}_\downarrow)\hat{\psi}^\dagger_{A,\uparrow}(\boldsymbol{\rho}_\uparrow) \times \hat{\psi}^\dagger_{A,\downarrow}(\boldsymbol{\rho}_\downarrow) + \mathrm{h.c.}, \tag{12}$$

$$\Delta(\boldsymbol{\rho}) = -\frac{k_F}{\sqrt{\pi}} \frac{J_z^2}{\delta} \phi_{\mathrm{rel}}(\boldsymbol{\rho}), \tag{13}$$

which describes a system of two-component fermions with an order parameter $\Delta(\boldsymbol{\rho})$. The latter has an s-wave symmetry inherited from the s-wave symmetry of the molecular wavefunction (see equation (3)). This scheme could be used to study low-dimensional Fermi gases with a superfluid gap applied externally.

## 3. Creating a topological superfluid

The technique of proximity-induced superfluid gap presented in section 2 can be used to create a topological superfluid. For simplicity, in this section we restrict the discussion to the limit of perturbative coupling to the mBEC for which the atom dynamics is restricted to plane $A$.

Optical lattices along $x$ and $y$ are applied to plane $A$ only. The $y$ lattice freezes the motion along $y$, leading to a quasi-1D geometry. The $x$-lattice is a spin-dependent tight-binding optical lattice as described in figure 1(a): each spin state is held in a sublattice of period $2d$, with the two sublattices shifted by a distance $d$. This system can be viewed as a lattice of spacing $d$ with spin $\uparrow$ ($\downarrow$) particles localized in the even (odd) sites $2i$ ($2i+1$, respectively). The practical realization of this lattice structure is described in section 5.2.

The physical system restricted to the lowest band of the optical lattice can formally be viewed as a spin-polarized system of fermions on a discrete lattice. Expanding the fermionic field operators on the basis of Wannier functions:

$$\hat{\psi}^\dagger_{A,\uparrow}(\boldsymbol{\rho}) = \sum_i w_x(x - 2id) w_y(y) \hat{c}^\dagger_{2i}, \tag{14}$$

$$\hat{\psi}^\dagger_{A,\downarrow}(\boldsymbol{\rho}) = \sum_i w_x(x - (2i+1)d) w_y(y) \hat{c}^\dagger_{2i+1}, \tag{15}$$

we rewrite the Hamiltonian (12) as

$$\hat{H}^{(2)}_\Delta = \sum_{i,j} \Delta^{(2)}_{2i,2j+1} \hat{c}^\dagger_{2i} \hat{c}^\dagger_{2j+1} + \mathrm{h.c.}, \tag{16}$$

where

$$\Delta^{(2)}_{2i,2j+1} = -\frac{k_F}{\sqrt{\pi}} \frac{J_z^2}{\delta} \int \mathrm{d}\boldsymbol{\rho}_\uparrow \mathrm{d}\boldsymbol{\rho}_\downarrow \, \phi_{\mathrm{rel}}(\boldsymbol{\rho}_\uparrow - \boldsymbol{\rho}_\downarrow) w_y(y_\uparrow) w_y(y_\downarrow) \times w_x(x_\uparrow - 2id) w_x(x_\downarrow - (2j+1)d). \tag{17}$$

An analytic expression for $\Delta^{(2)}_{i,j}$ can be obtained assuming that the $1/e$ size $\sigma_x$ of the Wannier function along $x$ is much smaller than the lattice spacing $d$, and that the extent of the wavefunction along $y$ is much larger than the 2D scattering length $a$:

$$\Delta^{(2)}_{i,j} = -2\sqrt{\pi} \frac{J_z^2}{\delta} k_F \sigma_x \, \mathrm{e}^{-|i-j|d/a}. \tag{18}$$

In the following, we will use values for the scattering length $a = d/2$, for which $\Delta_{i,j}$ is strongly suppressed except for nearest-neighbour pairs of sites, leading to the Hamiltonian

$$\hat{H}^{(2)}_\Delta = \Delta^{(2)} \sum_i \hat{c}^\dagger_{2i}(\hat{c}^\dagger_{2i+1} + \hat{c}^\dagger_{2i-1}) + \mathrm{h.c.} = \Delta^{(2)} \sum_i (-1)^i \hat{c}^\dagger_i \hat{c}^\dagger_{i+1} + \mathrm{h.c.}, \tag{19}$$

where

$$\Delta^{(2)} \equiv \Delta^{(2)}_{i,i+1} = -2\sqrt{\pi} \frac{J_z^2}{\delta} k_F \sigma_x \, \mathrm{e}^{-d/a}. \tag{20}$$

This Hamiltonian differs from the gap term in Kitaev's model due to the $(-1)^i$ factors. However, the latter can be eliminated by redefining the operators $\hat{c}_i$ according to $\hat{c}_{2i} \to (-1)^i \hat{d}_{2i}$ and $\hat{c}_{2i+1} \to (-1)^i \hat{d}_{2i+1}$.

The complete Kitaev model

$$\hat{H}_{\text{Kitaev}} = \sum_i -\mu\left(\hat{d}_i^\dagger \hat{d}_i - \frac{1}{2}\right) - J(\hat{d}_i^\dagger \hat{d}_{i+1} + \text{h.c.}) + \Delta(\hat{d}_i^\dagger \hat{d}_{i+1}^\dagger + \text{h.c.}) \quad (21)$$

is then obtained by introducing a small additional energy offset $\mu$ of plane $A$ and inducing the required atom tunnelling $J$ between neighbouring sites. The latter is performed using Raman transitions that flip the atom spin, which induces atom tunnelling with the required phase $(-1)^i$ of the hopping operator $\hat{d}_i^\dagger \hat{d}_{i+1} = (-1)^i \hat{c}_i^\dagger \hat{c}_{i+1}$ expressed with the physical operators $\hat{c}_i$ [46]. The required laser setup is described in section 5.2.

## 4. Bogoliubov spectra and Majorana fermions

The topological character of a topological superfluid can be characterized by its spectrum of Bogoliubov excitations. Let us recall the main properties of Bogoliubov excitations in the case of Kitaev's model, which are the eigenenergies of the Bogoliubov Hamiltonian (1) [6]. In the case of a homogeneous 1D chain with periodic boundary conditions, the spectrum of Bogoliubov excitations is gapped when $\Delta > 0$, except when the chemical potential is fine-tuned to $\mu = -2J$ or $2J$. These points indicate phase transitions between topologically different configurations. The phase $\mu < -2J$ can be smoothly connected to the trivial vacuum by decreasing $\mu$ to $-\infty$ without closing the gap; it is thus non-topological. The phase $\mu > 2J$ is essentially equivalent to $\mu < -2J$ since both phases are related by a particle–hole transform. On the other hand, as shown in [6] the phase $-2J < \mu < 2J$ has a non-trivial topology, in the sense that it can be distinguished from the $|\mu| > 2J$ phase via a different value of a $\mathbb{Z}_2$ topological invariant defined in [6].

Similar to edge states in the topological quantum Hall phases, for a chain with open boundary conditions the non-trivial topology is associated with boundary states. In the case of 1D topological superfluids, the boundary states form a pair of Majorana modes occurring at zero energy, i.e. in the middle of the gap of bulk Bogoliubov excitations. These states are highly non-local—delocalized at both ends of the topological superfluid—and become exponentially degenerate when increasing the size of the topological phase.

We present in this section the spectra of Bogoliubov excitations calculated for realistic experimental parameters. The calculations are performed by direct diagonalization of a discretized version of the complete Bogoliubov Hamiltonian (see equation (10)), with the optical lattice configuration described in section 3. We use a system size of 30 to 60 $d$, with a discretization pixel size of $d/4$. The system parameters are the following: the lattice spacing $d$ is equal to half the wavelength $\lambda$ of the optical lattice (see section 5.2), and we choose a 2D scattering length value $a = d/2$ so that the proximity-induced gap is restricted to nearest neighbours. This scattering length value corresponds to a molecular binding energy $E_b \simeq 0.8\,E_r$, where $E_r = \hbar^2/2m\lambda^2$ denotes the recoil energy. The molecule density in $B$ is fixed to a value $n_{\text{mol}} = 0.16\,d^{-2}$ corresponding to a Fermi energy $E_F = E_b/4$, i.e. on the BEC side of the BEC-BCS crossover of s-wave Fermi superfluids. This condition ensures that at low temperature the condensed fraction of the mBEC tends to unity [51]. We choose an $x$-lattice depth value $V_x = 5\,E_r$, which leads to a spontaneous atom tunnelling of negligible amplitude $6.2 \times 10^{-4}\,E_r$. The band gap is then equal to $2.0\,E_r$, a value larger than the energy offset $\delta = E_b/2 = 0.4\,E_r$, as required by the single-band assumption made above.

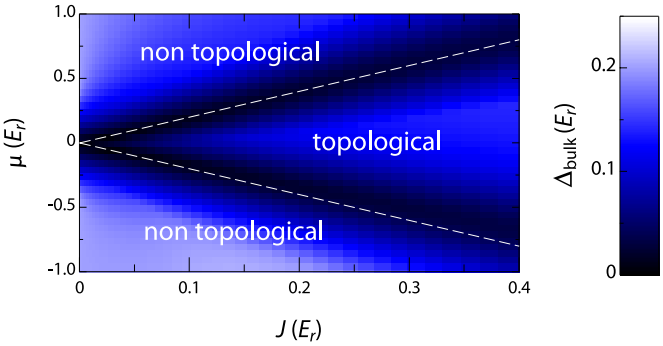


**Figure 2.** Amplitude of the bulk superfluid gap $\Delta_{\text{bulk}}$ as a function of the tunnel coupling $J$ and the chemical potential $\mu$ calculated for a system of 30 lattice sites with periodic boundary conditions. The topological transition corresponds to the lines for which the gap cancels; their location agrees well with the prediction of Kitaev's model $\mu = \pm 2J$ (dashed white lines).

For the Raman-induced tunnelling rate, we take a value of the order of the p-wave gap $\Delta^{(2)}$ calculated in second-order perturbation theory, which should maximize the system bulk gap $\Delta_{\text{bulk}}$ in the perturbative limit $J_z \ll \delta$ (more precisely $\Delta_{\text{bulk}} = 2\,\Delta$ for $J = \Delta$ for Kitaev's model [6]).

### 4.1. Homogeneous topological superfluid

We discuss in this section the case of a homogeneous system.

We first calculate the spectrum of Bogoliubov excitations for a homogeneous system of 30 lattice sites with periodic boundary conditions. The spectrum exhibits a bulk gap whose amplitude $\Delta_{\text{bulk}}$ is plotted in figure 2 as a function of the tunnel coupling $J$ and the chemical potential $\mu$. We observe a cancellation of the bulk gap on two lines of the phase diagram $\mu \simeq \pm 2J$, which is in agreement with the prediction of Kitaev's model. The lines indicate the location of the topological transition.

We then repeat the calculation of the Bogoliubov spectra for homogeneous systems with sharp boundaries, for which zero-energy Majorana end states are expected in the topological phase. We first consider a small tunnelling rate value $J_z = 0.2\,\delta$. As shown in figure 3(a), the calculated spectrum of Bogoliubov excitations is very similar to the one of Kitaev's lattice model, with a bulk gap and two Majorana states at zero energy. The full excitation spectrum quantitatively differs from Kitaev's model due to additional effects such as the creation of atom pairs in non-neighbouring lattice sites; yet the bulk gap value is in good agreement with the second-order perturbation result of equation (20).

When increasing the tunnelling rate value beyond the weak coupling regime $J_z \ll \delta$, we find that the structure of

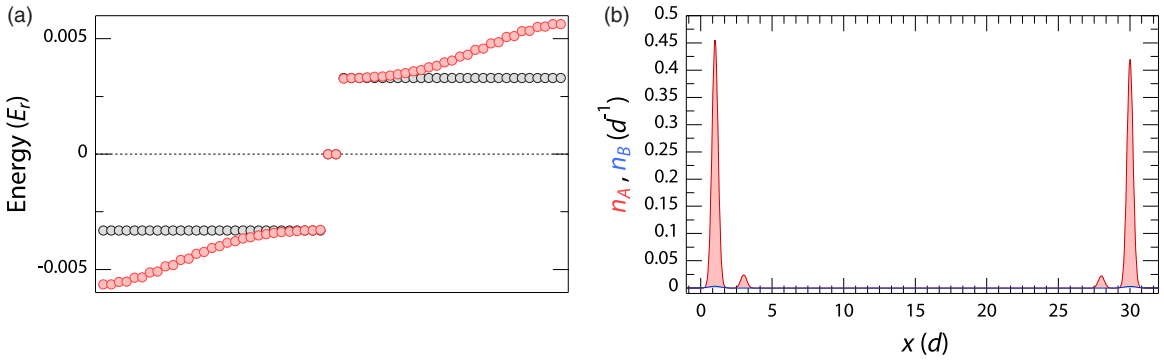


**Figure 3.** (a) Spectrum of Bogoliubov excitations (red dots) calculated for $J_z = 0.2\,\delta$ and $J = \Delta^{(2)}$, and compared with the prediction of Kitaev's model with $J = \Delta = \Delta^{(2)}$ (black dots). (b) Density distribution along $x$ of a zero-energy Majorana state, in planes $A$ (red line) and $B$ (blue line), revealing the non-local character of Majorana states. In the perturbative regime $J \ll \delta$, the population in $B$ remains small.

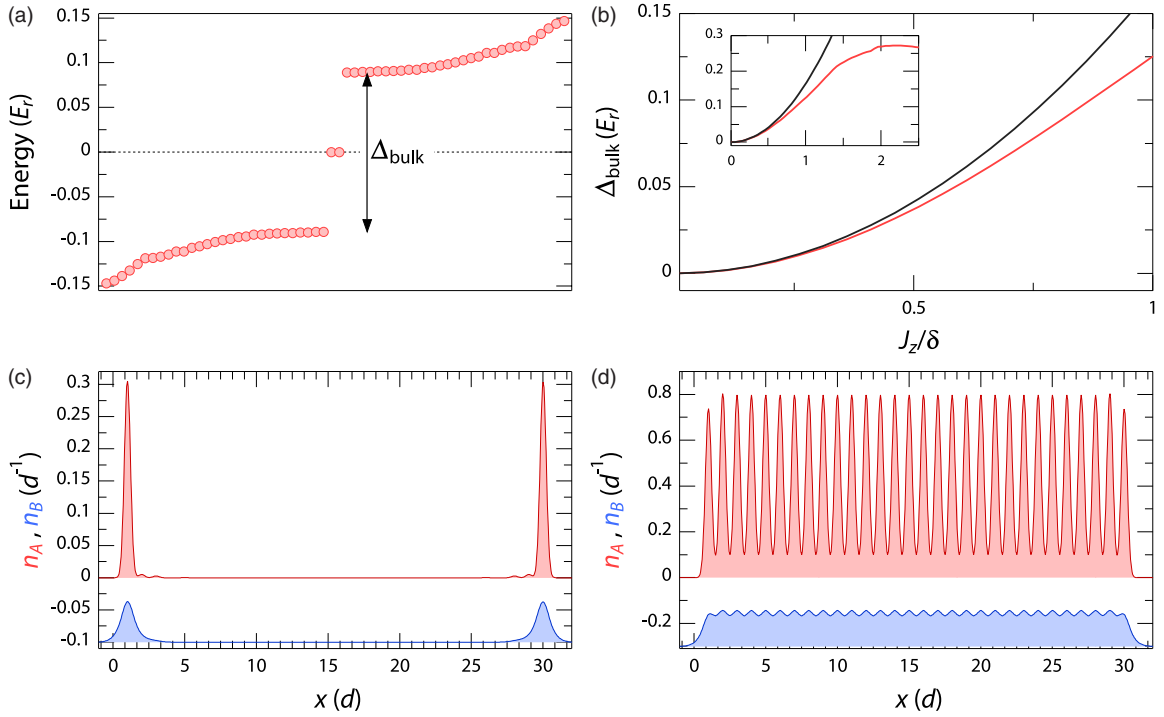


**Figure 4.** (a) Spectrum of Bogoliubov excitations (red dots) for a homogeneous system with sharp boundaries, calculated for $J_z = \delta$ and $J = 2\,\Delta^{(2)}$. It exhibits a bulk gap $\Delta_{\rm bulk} = 0.18\,E_r$ and a pair of zero-energy Majorana states with a residual splitting $\Delta_s \sim 10^{-12}\,E_r$. (b) Evolution of the bulk gap amplitude $\Delta_{\rm bulk}$ as a function of the ratio $J_z/\delta$ (red line), for $J = \Delta^{(2)}$, with $\Delta^{(2)}$ given by equation (20). The black line represents the prediction of second-order perturbation theory $\Delta_{\rm bulk} = 2\,\Delta^{(2)}$. (c) Density distribution along $x$ of a zero-energy Majorana state, in planes $A$ (red line) and $B$ (blue line, offset for clarity). In the strong coupling regime $J \sim \delta$, the population in $B$ is not negligible. (d) Total density distribution along $x$ calculated at zero temperature. Majorana states are not visible in this almost uniform density profile.

the Bogoliubov spectra qualitatively remains the same for tunnelling rates $J_z \sim \delta$ (see figure 4(a)). This should allow one to create p-wave superfluids with large bulk gap values $\Delta_{\rm bulk} \sim 0.2\,E_r$, which corresponds to a gap of $k_B \times 40$ nK for the physical system described in section 5 (see figure 4(b)). As the gas temperature has to be much smaller than the Fermi energy $E_F \simeq 0.2\,E_r$ in order to create a molecular BEC in plane $B$ [52], we expect the p-wave superfluid to be essentially in the zero-temperature regime for $J_z \sim \delta$.

The density probability of the Majorana states at zero energy is shown in figure 4(c) in the case $J_z = \delta$. In plane $A$ essentially only the lattice sites at the edge of the system are populated. We note that in that case the probability of occupying plane $B$ is not negligible (about 30%). The total atom density probability is almost uniform and close to half-filling (see figure 4(d)).

### *4.2. Topological superfluid in a harmonic trap*

Homogeneous systems with sharp boundaries are difficult to realize with ultracold atom systems. We thus now focus on gases held in a harmonic trap $V(x) = \frac{1}{2}m\omega^2x^2$. In a local density approximation picture, the local properties of the gas are expected to be close to the ones of a homogeneous gas with a local chemical potential $\mu - V(x)$. A gas of chemical potential $-2J < \mu < 2J$ should thus exhibit a

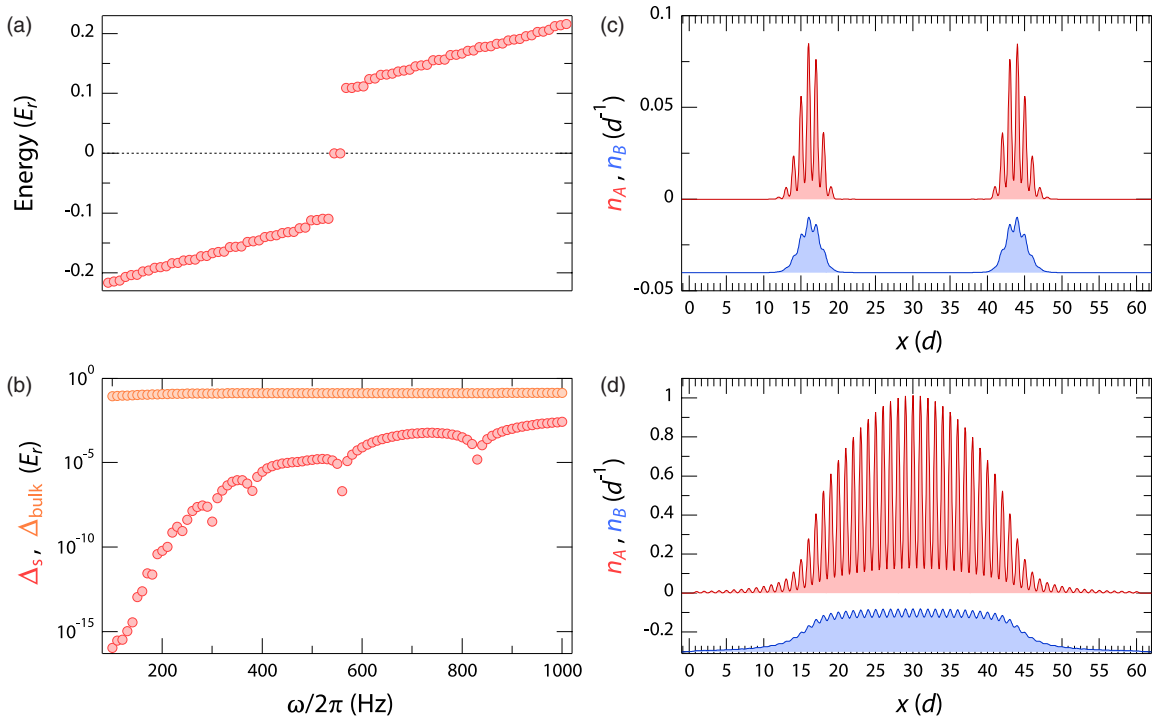


**Figure 5.** (a) Spectrum of Bogoliubov excitations (red dots) for a harmonically trapped system, calculated for $J_z = 1.5\,\delta, J = 2\,\Delta^{(2)}$, $\omega = 2\pi \times 200$ Hz. It exhibits a bulk gap $\Delta_{\rm bulk} = 0.22\,E_r$ and a pair of zero-energy Majorana states with a residual splitting $\Delta_s \sim 10^{-10}\,E_r$. (b) Evolution of the energy splitting $\Delta_s$ between Majorana states (red dots) and of the bulk gap $\Delta_{\rm bulk}$ (orange dots) as a function of the trapping frequency $\omega$. While the bulk gap essentially does not depend on $\omega$, the splitting between Majorana states strongly decreases when decreasing the $\omega$ value, i.e. increasing the separation between Majorana fermions. (c) Density distribution along $x$ of a zero-energy Majorana state, in planes $A$ (red line) and $B$ (blue line). (d) Total density distribution along $x$ calculated at zero temperature.

phase separation with a topological superfluid phase in the trap bottom ($\mu - V(x) > -2J$) and trivial superfluids at the edges ($\mu - V(x) < -2J$). We also expect the presence of Majorana zero-energy states at the boundary of the topological superfluid.

For the parameters given in the caption of figure 5, the calculated spectrum of the Bogoliubov excitations is gapped with a pair of quasi-degenerate Majorana end states at zero energy (see figure 5(a)). These states are non-local, being the superposition of two localized wavefunctions ($1/e$ size of $\simeq 2.5\,d$) separated by $\simeq 21\,d$ (see figure 5(c)). The position of these zero-energy modes agrees well with the position of the topological transition given by the local density approximation. Note that the Majorana states are not directly visible in the total density profile; yet at the location of the topological transition, the gas compressibility sharply varies (see figure 5(d)), which could be useful to establish the phase diagram of the system [53, 54].

A figure of merit of the topological protection can be given by the residual splitting between the two Majorana states. As shown in figure 5(b), the topological protection improves by increasing the separation between the Majorana fermions [55–57], which can be performed by opening the trap along $x$.

### *4.3. Probing the Majorana fermions*

As shown in figures 5(c) and (d), the presence of Majorana end states cannot be revealed from the total atom density. Photo-emission spectroscopy [58], which directly addresses the structure of the Bogoliubov excitation spectrum, is a convenient probe for these states [26, 27]. It consists here in coherently coupling the spin $|\uparrow\rangle$ atoms to an unpopulated internal state $|\alpha\rangle$, which can be probed either *in situ* or after time of flight. This coupling is described by the Hamiltonian $\hat{V} = V_0 e^{i\Omega t} \int dx\, \hat{\psi}_\alpha^\dagger(x)\hat{\psi}_\uparrow(x) + \text{h.c.}$, where $\hat{\psi}_\alpha^\dagger(x)$ creates a particle in the state $\|\alpha\rangle$ at the position $x$. The photoemission performed at a given frequency $\Omega$ gives rise to a transfer of atoms occupying the Bogoliubov excitations of energy $E$ matching the resonance condition $\hbar\Omega = \hbar\omega_0 - E$, where $\omega_0$ is the resonance frequency for a single atom. The energy of the final state $|\alpha\rangle$ is neglected for simplicity.

*4.3.1. Density probability of Majorana states.* In order to probe the density probability of Majorana states, we probe the target state density distribution right after the photoemission pulse. The target spin state $|\alpha\rangle$ can be chosen as another Zeeman state that would be trapped in the $x$ lattice, with a photoemission coupling provided by a radiofrequency field. We assume that the photoemission spectroscopy is performed in the linear perturbative regime, and that the target spin state $|\alpha\rangle$ can be imaged *in situ* with single-atom sensitivity [59, 60]. The density probability of $|\alpha\rangle$ atoms $n_\alpha(x) = \langle\hat{\psi}_\alpha^\dagger(x)\hat{\psi}_\alpha(x)\rangle$ as a function of the driving frequency is shown in figure 6. The bulk Bogoliubov excitations are associated with a broad energy spectrum above the superfluid gap. The Majorana boundary states correspond to a narrow feature at zero energy, with photoemitted atoms located at both ends of the topological superfluid phase.

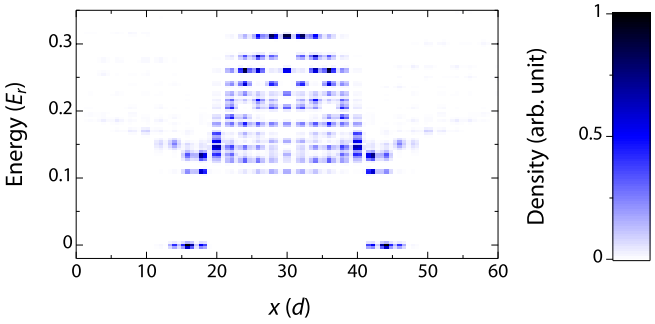


**Figure 6.** Position-resolved photoemission spectrum calculated with the parameters of figure 5. The Majorana states probed at zero energy are localized at the edges of the topological superfluid.

*4.3.2. Momentum distribution of Majorana states.* The photoemission technique can also be applied to extract the momentum distribution of Majorana states, by imaging the target state $|\alpha\rangle$ after time of flight.

For this measurement, the target state $|\alpha\rangle$ should be untrapped so that its eigenstates have a well-defined momentum. A possible choice for $|\alpha\rangle$ is a long-lived excited state[2], for which the optical dipole force of wavelength $\lambda$ used for the optical lattice would be very weak [62]. The photoemission coupling would be achieved using the ultranarrow optical transition between the ground electronic state and the state $|\alpha\rangle$.

The expected photoemission spectrum (shown in figure 7(a)) can be divided into a broad spectrum of bulk excitations and a narrow feature at zero energy corresponding to the Majorana states. The oscillatory behaviour at zero energy reflects the quantum superposition of the wavefunction of Majorana states at both ends of the topological superfluid. Besides demonstrating the non-local character of the Majorana states, this probe also allows one to discriminate between the two zero-energy states, whose phase of the interference pattern differs (shown in figure 7(b)).

*4.3.3. Adiabatic preparation of a given Majorana state.* In the previous section, we described how to discriminate between Majorana states using momentum-resolved photoemission spectroscopy. This raises the question of the preparation of the system in a given Majorana state [26], which is an important prerequisite for the manipulation of Majorana fermions for quantum information purposes. We propose to prepare a given Majorana state by crossing adiabatically a phase transition from a trivial to a topological superfluid phase. This can be achieved by changing adiabatically the chemical potential $\mu$, which can be performed by dynamically varying the double-well energy offset (see section 5.2.1).

In the local density approximation framework, one expects a topological superfluid phase to nucleate in the trap bottom when the chemical potential corresponds to the critical value for topological superfluidity $\mu_c$ at the bottom of the trap ($\mu_c \simeq -2J$). As shown in figure 8(a), the nucleation of the topological superfluid is associated with the creation of Majorana zero-energy states from two bulk states (one from the hole sector, and one from the particle sector) when increasing the chemical potential value across $\mu = \mu_c$. By increasing adiabatically the chemical potential value from a trivial to a topological phase, one thus expects the system to populate the Majorana state which is adiabatically connected to the hole sector of the trivial superfluid. In order to test the feasibility of this scheme, we simulated the effect of the finite duration of the chemical potential ramp [63, 64]. For this, we numerically solved the Schrödinger equation using the Bogoliubov Hamiltonian used in previous calculations, with a time-dependent chemical potential. As shown in figure 8(b), fidelities $\mathcal{F} > 0.9$ can be achieved with the parameters described in the caption of figure 8 for ramp durations of about 120 ms. Note that shorter adiabatic paths could be used if one crosses the topological transition with a lower atom number in plane $A$ (i.e. higher trapping frequency $\omega$), and then increases the atom number in $A$ by opening the trap far from the topological transition so that the Majorana states are deeply topologically protected.

## 5. Description of the experimental setup

### 5.1. Choice of the atomic species

The proposal described above makes use of a spin-dependent optical lattice potential. For fermionic alkali atoms ($^6$Li and $^{40}$K), spin-dependent optical dipole potentials are associated with large heating rates due to spontaneous emission [31, 32], because of the small fine-structure splitting of the $P$ electronic levels compared to the transition linewidth. In order to circumvent this issue, we propose to use a fermionic atom of the Lanthanide family, such as $^{167}$Er or $^{161}$Dy [65–67]. These atoms benefit from narrow optical transitions that can be used to create spin-dependent dipole potentials with small heating rates. For example, strong spin-dependent potentials can be created for Dy atoms using optical lattices at $\lambda = 530$ nm, close to the 530.3 nm transition (electronic angular momenta $J = 8 \rightarrow J' = 7$, linewidth $\Gamma = 2\pi \times 184$ kHz).

Due to the large magnetic moment of these atoms, we expect large dipolar relaxation rates, except for mixtures of the two Zeeman states of lowest energy in the case of a fermionic species [68]. As shown in the case of $^{168}$Er BECs, the very large number of Zeeman states in the electronic ground state should lead to numerous Feshbach resonances, making it possible to create a molecular BEC for large scattering length values [67].

### 5.2. Optical lattice configuration

We describe in this section the laser configuration required to create the double-well potential along $z$, the plane-dependent lattices along $x$ and $y$, and the Raman lasers driving atom tunnelling in the $x$ lattice.

*5.2.1. Superlattice potential along z.* The atoms are confined in a bilayer system of two planes $A$ and $B$ using a double-well

[2] Such as the $4f^9(^6H^0)5d6s^2\ ^7H_8^0$ metastable state of Dy ($1/e$ lifetime of 7 ms), coupled to the ground electronic state by an optical transition at 1322 nm [61].

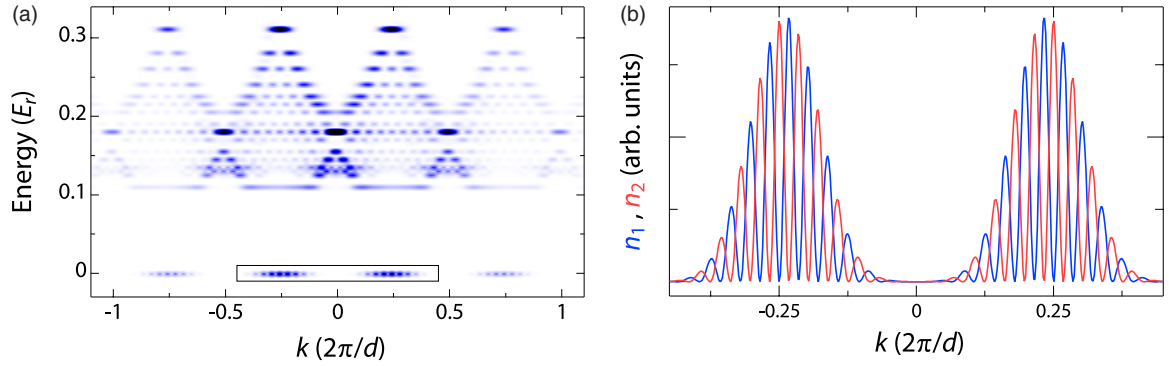


**Figure 7.** (a) Momentum-resolved photoemission spectrum, exhibiting an oscillatory behaviour at zero energy reflecting the delocalization of the Majorana states at both ends of the topological superfluid. The small rectangle at zero energy represents the spectrum of the Majorana states shown in (b). (b) Momentum-resolved photoemission spectrum $n_i(k)$ for both Majorana states $i = 1, 2$, differing from the phase of the fast oscillations. The slow modulation (period $\pi/\mathrm{d}$) reflects the wavefunction modulation by the lattice potential, while the fast oscillation is due to the delocalization of the wavefunction at both ends of the topological superfluid.

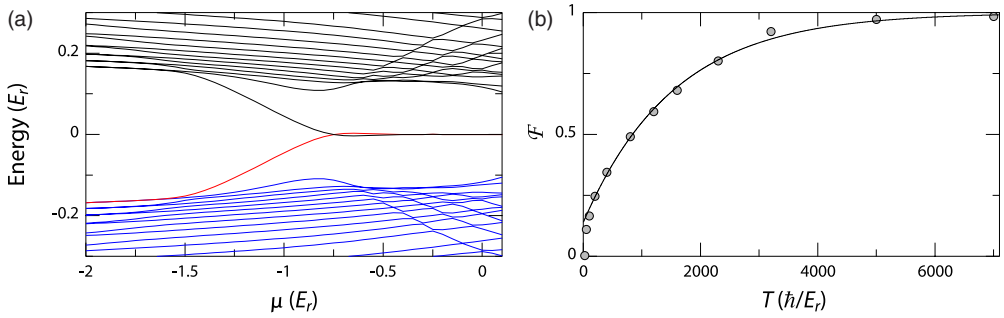


**Figure 8.** (a) Energy of the Bogoliubov excitations as a function of the chemical potential $\mu$. The parameters are the same as for figure 5, expect with a trap frequency $\omega/2\pi = 600\,\mathrm{Hz}$. The bulk hole sector is pictured in blue. Starting with a system prepared at low temperature in the trivial phase ($\mu \simeq -2\,E_r$), the Majorana state connected to the hole sector of the trivial superfluid (in red) can be prepared by increasing adiabatically the chemical potential up to $\mu = 0$. (b) Expected fidelity $\mathcal{F}$ as a function of the ramp duration $T$ (black dots). The solid line is an exponential fit to the numerical data. A fidelity $\mathcal{F} > 0.9$ is expected for ramp durations $T > 3300\,\hbar/E_r \simeq 120\,\mathrm{ms}$.

potential. The latter can be created using a bichromatic optical lattice along $z$, i.e. the superposition of two standing waves of wavelength $\lambda$ and $2\lambda$, leading to a potential

$$V_{\mathrm{SL}}(z) = V_1 \cos^2(kz) + V_2 \cos^2(kz/2 + \phi), \tag{22}$$

where $k = 2\pi/\lambda$ [69] (see figure 9(a)). Atom tunnelling towards other planes is suppressed using lattice depths of about $20\,E_r$. The lattice intensities $V_1, V_2$ and relative phase $\phi$ enable one to control independently the tunnel coupling $J_z$ between $A$ and $B$ and the value of the energy offsets $\delta$ and $\mu$.

*5.2.2. Plane-dependent lattices along x and y.* An optical lattice is used to freeze the atom motion along $y$ in plane $A$. The atom motion in plane $B$, which contains the two-dimensional mBEC, should remain unaffected so that phase coherence in the mBEC is maintained.

The plane-dependent optical lattice along $y$ can be created using the interference of a travelling wave propagating along $\mathbf{u} = \cos\alpha\,\mathbf{e_y} + \sin\alpha\,\mathbf{e_z}$ with a standing wave along $z$ (see figure 10(c)), creating a potential

$$V(\mathbf{r}) \propto |E_u e^{\mathrm{i}k\mathbf{u}_\mathbf{y}\cdot\mathbf{r}} + E_z \cos(kz + \phi')|^2 \tag{23}$$

$$= |E_z|^2 \cos^2(kz + \phi') + 2|E_z E_u| \cos(kz + \phi') \cos(k(\cos\alpha\, y + \sin\alpha\, z)) + |E_u|^2. \tag{24}$$

The first term represents a simple optical lattice along $z$ that contributes to the superlattice potential. The second term consists of an optical lattice along $y$ of lattice spacing $d_y = \lambda/\cos\alpha$ whose amplitude depends on the plane positions $z_A$ and $z_B$. As the $z$ standing wave has a node on the retroreflection mirror, the phase $\phi'$ can be controlled with high precision by varying the laser frequency over typically a GHz range [69, 70]. This allows one to choose the value of $\phi'$ so that the $y$ lattice amplitude vanishes at $z_B$, leaving the motion of molecules in plane $B$ unaffected (see figures 9(b) and (c)).

Choosing the value $\alpha = \pi/3$ corresponds to a $y$ lattice spacing $d_y = 2\,\lambda$. For such a value $d_y \gg a$, the amplitude for atom pair tunnelling into different tubes is about $10^{-3}$ smaller than for pair tunnelling into the same tube. This allows one to consider that the tubes are independent from each other.

The same technique can be used to create the lattice potential along $x$. As the optical lattice wavelength is chosen close to a narrow transition, vector light shifts can be used to create the spin-dependent potential in the desired configuration shown in figure 10(b). We checked that using specific laser polarizations, we can create the required spin-independent lattices along $y$ and $z$ and the spin-dependent lattice along $x$ (see appendix B).

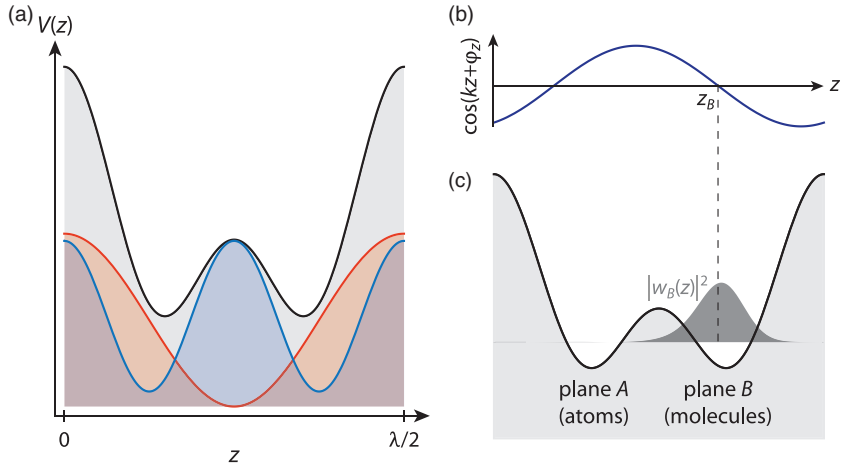


**Figure 9.** (a) Scheme of the bichromatic superlattice potential along $z$ (black line), made of the superposition of two standing waves of wavelength $\lambda$ (blue line) and $2\lambda$ (red line). The energy offset $\delta$ in the resulting double-well potential can be controlled using a relative offset in position of the two standing waves. (b) Amplitude of the standing wave along $z$ used for generating the $y$ lattice, which vanishes at $z_B$. (c) Superlattice potential with the Wannier function in plane $B$ centred on $z_B$.

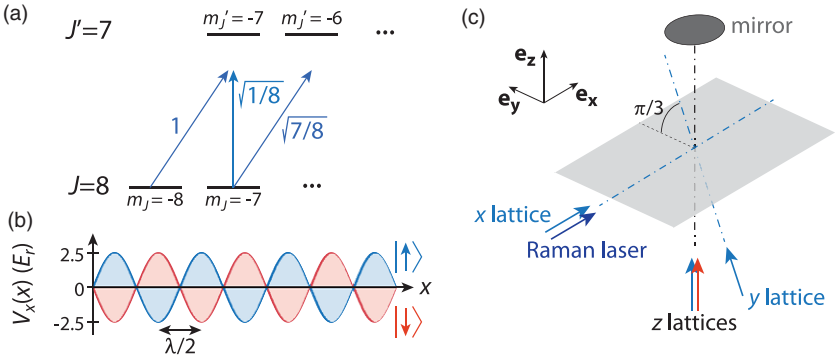


**Figure 10.** (a) Scheme of the electronic states used for creating spin-dependent optical lattices with a $J \to J' = J - 1$ optical transition. (b) Lattice potential along $x$ obtained by interfering a standing wave along $z$ with a plane wave along $x$. The required spin-dependent lattice configuration is achieved for specific choices of polarization. (c) Geometry of the complete laser configuration generating the optical lattice potential and the laser-induced tunnelling in the $x$ lattice.

*5.2.3. Laser-induced tunnelling.* In order to realize Kitaev's model, atom tunnelling in the $x$ lattice should be described by the Hamiltonian $-J\sum_i(-1)^i\hat{c}_i^\dagger\hat{c}_{i+1}$. The required alternation of the sign of the tunnel amplitude can be achieved by inducing atom tunnelling via Raman transitions in the following geometry (see figure 10(c)): one of the Raman beams would be the $z$ lattice beam used for generating the $x$ and $y$ lattices, and the second beam would propagate along $x$, with a frequency detuning equal to the $|\uparrow\rangle \leftrightarrow |\downarrow\rangle$ transition frequency. The hopping matrix element between the sites $2i$ and $2i+1$ is then given by

$$J_{2i,2i\pm1} = \hbar\Omega_0 \int \mathrm{d}\mathbf{r}\, \cos(kz+\phi_z)\, \mathrm{e}^{\mathrm{i}kx} W_{2i}(\mathbf{r})^* W_{2i\pm1}(\mathbf{r}), \quad (25)$$

where $W_i(\mathbf{r}) = w_x(x-id)w_y(y)w_z(z)$ is the Wannier function of the site $i$ of the $x$ lattice and $\Omega_0$ is the Rabi frequency of the Raman transition in vacuum. An explicit calculation leads to the result

$$J_{2i,2i\pm1} = \pm J,$$

$$J = \hbar\Omega_0 \int \mathrm{d}z\, \cos(kz+\phi_z)|w_z(z)|^2 \times \int \mathrm{d}x\, \mathrm{e}^{\mathrm{i}kx} w_x(x)^* w_x(x-d), \quad (26)$$

which is the desired configuration, assuming the gauge is chosen so that $J$ is real.

## 6. Conclusions and perspectives

In this paper, we have discussed how to realize 1D topological superfluids with ultracold Fermi gases. We described how to probe the Majorana fermions located at the edges of the topological superfluid phase. Further developments could address the robustness of the Majorana degeneracy with respect to disorder [71, 72] and atomic interactions between neighbouring sites [73–76], which could be induced by the large dipole–dipole interactions for Dy or Er atoms[3]. On a longer term the manipulation of Majorana fermions would allow one to exhibit their non-Abelian statistics, which is the basic ingredient for developing topological quantum computation [77–79]. The realization of braiding operations requires either implementing a network of coupled 1D tubes [80] or creating a two-dimensional $p_x + \mathrm{i}p_y$ topological

[3] For two Dy atoms separated by $\lambda/2 = 265$ nm the dipole–dipole interaction varies between $-0.03\,E_r$ and $0.016\,E_r$, depending on the magnetic field direction.

superfluid with Majorana fermions bound to half-quantum vortices [4, 79, 81]. The experimental scheme presented in this paper could be adapted to a 2D geometry to realize a lattice $p_x + \mathrm{i}p_y$ topological superfluid.

## Acknowledgments

We thank the members of the 'Bose–Einstein condensates' and 'Fermi gases' groups at LKB, the Quantum optics theory group at Innsbruck university, V Gurarie, N Cooper, and N Goldman for helpful discussions. Laboratoire Kastler Brossel is unité mixte de recherche (UMR 8552) of the CNRS.

## Appendix A. Semi-classical approximation

In this appendix, we provide details on the calculation of the proximity-induced gap using a semi-classical approximation. For replacing the mBEC coherent state by a classical field, we use a unitary displacement of the Hamiltonian by the operator $\hat{D}_{\mathrm{mBEC}} = \mathrm{e}^{-\sqrt{\mathrm{N}}/2}\exp(\sqrt{\mathrm{N}}(\hat{\psi}^{\dagger}_{\mathrm{mol}} - \hat{\psi}_{\mathrm{mol}}))$. For the calculation of $\hat{D}^{\dagger}_{\mathrm{mBEC}}\hat{H}_z\hat{D}_{\mathrm{mBEC}}$ we use the formula

$$\mathrm{e}^{\hat{A}}\hat{B}\,\mathrm{e}^{-\hat{A}} = \hat{B} + [\hat{A},\hat{B}] + \frac{1}{2!}[\hat{A},[\hat{A},\hat{B}]] + \frac{1}{3!}[\hat{A},[\hat{A},[\hat{A},\hat{B}]]] + \cdots. \tag{A.1}$$

This leads to an effective Hamiltonian

$$\begin{aligned}\hat{H}_{\mathrm{eff}} = &-J_z\int \mathrm{d}\boldsymbol{\rho}\,\mathrm{d}\boldsymbol{\rho}'\, f(\boldsymbol{\rho}'-\boldsymbol{\rho}')\\ &\left(\hat{\psi}^{\dagger}_{A,\uparrow}(\boldsymbol{\rho})\hat{\psi}_{B,\uparrow}(\boldsymbol{\rho}') + \hat{\psi}^{\dagger}_{A,\downarrow}(\boldsymbol{\rho})\hat{\psi}_{B,\downarrow}(\boldsymbol{\rho}') + \mathrm{h.c.}\right)\\ &- J_z\int \mathrm{d}\boldsymbol{\rho}_{\uparrow}\mathrm{d}\boldsymbol{\rho}_{\downarrow}\, g(\boldsymbol{\rho}_{\uparrow}-\boldsymbol{\rho}_{\uparrow})\\ &\left(\hat{\psi}^{\dagger}_{B,\uparrow}(\boldsymbol{\rho}_{\uparrow})\hat{\psi}^{\dagger}_{A,\downarrow}(\boldsymbol{\rho}_{\downarrow}) + \hat{\psi}^{\dagger}_{A,\uparrow}(\boldsymbol{\rho}_{\uparrow})\hat{\psi}^{\dagger}_{B,\downarrow}(\boldsymbol{\rho}_{\downarrow}) + \mathrm{h.c.}\right),\end{aligned}$$

where the first term describes atom tunnelling between planes $A$ and $B$ and the second term corresponds to the creation/annihilation of atom pairs from the mBEC.

The functions $f(\rho)$ and $g(\rho)$ are given by

$$f(\rho) = \delta(\rho) + \sum_{n=1}^{\infty}\frac{(-1)^n}{(2n)!}\left(\frac{k_F a}{2\pi}\right)^{2n} K_0^{*2n}(\rho), \tag{A.2}$$

$$g(\rho) = \sum_{n=0}^{\infty}\frac{(-1)^{n+1}}{(2n+1)!}\left(\frac{k_F a}{2\pi}\right)^{2n+1} K_0^{*2n+1}(\rho), \tag{A.3}$$

where $K_0^{*i}$ refers to the function $K_0$ convolved with itself $i$ times.

In the main text, we only kept for both functions the first term of the series. We checked that for the value $E_F = E_b/4$ used for the calculations this assumption is justified (error on $g(\rho)$ smaller than 10%).

## Appendix B. Polarization of the optical lattices

We provide in table B1 a possible choice for the polarization of the lasers used for the spin-independent lattices along $z$ and $y$, and the spin-dependent lattice along $x$.

**Table B1.** Table of numerical values for the magnetic field direction and laser directions/polarizations leading to spin-independent lattices along $z$ and $y$, and a spin-dependent lattice along $x$ in the required configuration.

| | Direction | Polarization |
|---|---|---|
| $B$ field | $\mathbf{u}_B = \cos\beta\,\mathbf{e_y} + \sin\beta\,\mathbf{e_z}$, $\beta = 0.43$ rad | |
| $z$ standing wave | $\mathbf{e_z}$ | $\cos\theta_z\,\mathbf{e_x} + \mathrm{i}\sin\theta_z\,\mathbf{e_y}$, $\theta_z = 0.86$ rad |
| $x$ travelling wave | $\mathbf{e_x}$ | $\cos\theta_x\,\mathbf{e_y} + \sin\theta_x\,\mathbf{e_z}$, $\theta_x = 0.53$ rad |
| $y$ travelling wave | $\mathbf{u}_y = \cos\alpha\,\mathbf{e_y} + \sin\alpha\,\mathbf{e_z}$, $\alpha = \pi/3$ | $\cos\theta_y\,\mathbf{e_x} \times \mathbf{u_y} + \sin\theta_y\,\mathbf{e_x}$, $\theta_y = 1.05$ rad |

## References

[1] Hasan M Z and Kane C L 2010 Colloquium: topological insulators *Rev. Mod. Phys.* **82** 3045
[2] Qi X L and Zhang S C 2011 Topological insulators and superconductors *Rev. Mod. Phys.* **83** 1057
[3] Volovik G E 2003 *The Universe in a Helium Droplet* vol 117 (New York: Oxford University Press)
[4] Read N and Green D 2000 Paired states of fermions in two dimensions with breaking of parity and time-reversal symmetries and the fractional quantum Hall effect *Phys. Rev.* B **61** 10267
[5] Kopnin N B and Salomaa M M 1991 Mutual friction in superfluid $^3$He: effects of bound states in the vortex core *Phys. Rev.* B **44** 9667
[6] Kitaev A Y 2001 Unpaired Majorana fermions in quantum wires *Phys.—Usp.* **44** 131
[7] Teo J C Y and Kane C L 2010 Topological defects and gapless modes in insulators and superconductors *Phys. Rev.* B **82** 115120
[8] Essin A M and Gurarie V 2011 Bulk-boundary correspondence of topological insulators from their respective Green's functions *Phys. Rev.* B **84** 125132
[9] Majorana E 1937 Teoria simmetrica dell'elettrone e del positrone *Nuovo Cimento* **14** 171–84
[10] Fu L and Kane C L 2008 Superconducting proximity effect and Majorana fermions at the surface of a topological insulator *Phys. Rev. Lett.* **100** 096407
[11] Lutchyn R M, Sau J D and Das Sarma S 2010 Majorana fermions and a topological phase transition in semiconductor–superconductor heterostructures *Phys. Rev. Lett.* **105** 77001
[12] Oreg Y, Refael G and Von Oppen F 2010 Helical liquids and Majorana bound states in quantum wires *Phys. Rev. Lett.* **105** 177002
[13] Beenakker C W J 2011 Search for Majorana fermions in superconductors arXiv:1112.1950
[14] Alicea J 2012 New directions in the pursuit of Majorana fermions in solid state systems *Rep. Prog. Phys.* **75** 076501
[15] Mourik V, Zuo K, Frolov S M, Plissard S R, Bakkers E and Kouwenhoven L P 2012 Signatures of Majorana fermions in hybrid superconductor-semiconductor nanowire devices *Science* **336** 1003–7
[16] Williams J R, Bestwick A J, Gallagher P, Hong S S, Cui Y, Bleich A S, Analytis J G, Fisher I R and Goldhaber-Gordon D 2012 Unconventional Josephson effect in hybrid superconductor-topological insulator devices *Phys. Rev. Lett.* **109** 56803
[17] Rokhinson L P, Liu X and Furdyna J K 2012 Observation of the fractional ac Josephson effect: the signature of Majorana particles arXiv:1204.4212

[18] Deng M T, Yu C L, Huang G Y, Larsson M, Caroff P and Xu H Q 2012 Observation of Majorana fermions in a Nb-InSb nanowire-Nb hybrid quantum device arXiv:1204.4130

[19] Gurarie V, Radzihovsky L and Andreev A V 2005 Quantum phase transitions across a p-wave Feshbach resonance *Phys. Rev. Lett.* **94** 230403

[20] Cooper N R and Shlyapnikov G V 2009 Stable topological superfluid phase of ultracold polar fermionic molecules *Phys. Rev. Lett.* **103** 155302

[21] Levinsen J, Cooper N R and Shlyapnikov G V 2011 Topological $p_x + ip_y$ superfluid phase of fermionic polar molecules *Phys. Rev.* A **84** 013603

[22] Stanescu T D, Galitski V and Sarma S D 2010 Topological states in two-dimensional optical lattices *Phys. Rev.* A **82** 013608

[23] Jiang L, Kitagawa T, Alicea J, Akhmerov A R, Pekker D, Refael G, Cirac J I, Demler E, Lukin M D and Zoller P 2011 Majorana fermions in equilibrium and in driven cold-atom quantum wires *Phys. Rev. Lett.* **106** 220402

[24] Diehl S, Rico E, Baranov M A and Zoller P 2011 Topology by dissipation in atomic quantum wires *Nature Phys.* **7** 971–7

[25] Bloch I, Dalibard J and Zwerger W 2008 Many-body physics with ultracold gases *Rev. Mod. Phys.* **80** 885

[26] Kraus C V, Diehl S, Zoller P and Baranov M A 2012 Probing atomic Majorana fermions in optical lattices arXiv:1201.3253

[27] Liu X J, Jiang L, Pu H and Hu H 2012 Probing Majorana fermions in spin–orbit-coupled atomic Fermi gases *Phys. Rev.* A **85** 021603

[28] Regal C A, Ticknor C, Bohn J L and Jin D S 2003 Tuning p-wave interactions in an ultracold Fermi gas of atoms *Phys. Rev. Lett.* **90** 053201

[29] Zhang J, Van Kempen E G M, Bourdel T, Khaykovich L, Cubizolles J, Chevy F, Teichmann M, Tarruell L, Kokkelmans S and Salomon C 2004 p-wave Feshbach resonances of ultracold $^6$Li *Phys. Rev.* A **70** 030702

[30] Lin Y J, Jiménez-García K and Spielman I B 2011 Spin–orbit-coupled Bose–Einstein condensates *Nature* **471** 83–6

[31] Wang P, Yu Z Q, Fu Z, Miao J, Huang L, Chai S, Zhai H and Zhang J 2012 Spin–orbit coupled degenerate Fermi gases *Phys. Rev. Lett.* **109** 95301

[32] Cheuk L W, Sommer A T, Hadzibabic Z, Yefsah T, Bakr W S and Zwierlein M W 2012 Spin-injection spectroscopy of a spin–orbit coupled Fermi gas *Phys. Rev. Lett.* **109** 95302

[33] Zhang C, Tewari S, Lutchyn R M and Das Sarma S 2008 $p_x + ip_y$ superfluid from s-wave interactions of fermionic cold atoms *Phys. Rev. Lett.* **101** 160401

[34] Sato M, Takahashi Y and Fujimoto S 2009 Non-Abelian topological order in s-wave superfluids of ultracold fermionic atoms *Phys. Rev. Lett.* **103** 020401

[35] Gong M, Tewari S and Zhang C 2011 BCS-BEC crossover and topological phase transition in 3D spin–orbit coupled degenerate Fermi gases *Phys. Rev. Lett.* **107** 195303

[36] McMillan W L 1968 Tunneling model of the superconducting proximity effect *Phys. Rev.* **175** 537

[37] Martiyanov K, Makhalov V and Turlapov A 2010 Observation of a two-dimensional Fermi gas of atoms *Phys. Rev. Lett.* **105** 30404

[38] Dyke P, Kuhnle E D, Whitlock S, Hu H, Mark M, Hoinka S, Lingham M, Hannaford P and Vale C J 2011 Crossover from 2D to 3D in a weakly interacting Fermi gas *Phys. Rev. Lett.* **106** 105304

[39] Fröhlich B, Feld M, Vogt E, Koschorreck M, Zwerger W and Köhl M 2011 Radio-frequency spectroscopy of a strongly interacting two-dimensional Fermi gas *Phys. Rev. Lett.* **106** 105301

[40] Sommer A T, Cheuk L W, Ku M J H, Bakr W S and Zwierlein M W 2012 Evolution of fermion pairing from three to two dimensions *Phys. Rev. Lett.* **108** 045302

[41] Mandel O, Greiner M, Widera A, Rom T, Hänsch T W and Bloch I 2003 Coherent transport of neutral atoms in spin-dependent optical lattice potentials *Phys. Rev. Lett.* **91** 10407

[42] Lee P J, Anderlini M, Brown B L, Sebby-Strabley J, Phillips W D and Porto J V 2007 Sublattice addressing and spin-dependent motion of atoms in a double-well lattice *Phys. Rev. Lett.* **99** 20402

[43] McKay D and DeMarco B 2010 Thermometry with spin-dependent lattices *New J. Phys.* **12** 055013

[44] Soltan-Panahi P, Struck J, Hauke P, Bick A, Plenkers W, Meineke G, Becker C, Windpassinger P, Lewenstein M and Sengstock K 2011 Multi-component quantum gases in spin-dependent hexagonal lattices *Nature Phys.* **7** 434–40

[45] Karski M, Förster L, Choi J M, Alberti A, Alt W, Widera A and Meschede D 2011 Direct observation and analysis of spin dependent transport of single atoms in a 1d optical lattice *J. Korean Phys. Soc.* **59** 2947

[46] Jaksch D and Zoller P 2003 Creation of effective magnetic fields in optical lattices: the Hofstadter butterfly for cold neutral atoms *New J. Phys.* **5** 56

[47] Aidelsburger M, Atala M, Nascimbène S, Trotzky S, Chen Y A and Bloch I 2011 Experimental realization of strong effective magnetic fields in an optical lattice *Phys. Rev. Lett.* **107** 255301

[48] Petrov D S and Shlyapnikov G V 2001 Interatomic collisions in a tightly confined Bose gas *Phys. Rev.* A **64** 012706

[49] Glauber R J 1963 Coherent and incoherent states of the radiation field *Phys. Rev.* **131** 2766–88

[50] Avan P, Cohen-Tannoudji C, Dupont-Roc J and Fabre C 1976 Effect of high frequency irradiation on the dynamical properties of weakly bound electrons *J. Phys. B: At. Mol. Phys.* **37** 993–1009

[51] Salasnich L 2007 Condensate fraction of a two-dimensional attractive Fermi gas *Phys. Rev.* A **76** 015601

[52] Petrov D S, Baranov M A and Shlyapnikov G V 2003 Superfluid transition in quasi-two-dimensional Fermi gases *Phys. Rev.* A **67** 031601

[53] Liu X-J and Hu H 2012 Topological superfluid in one-dimensional spin–orbit-coupled atomic Fermi gases *Phys. Rev.* A **85** 033622

[54] Seo K, Han L and Sá de Melo C A R 2012 Topological phase transitions in ultracold Fermi superfluids: the evolution from Bardeen–Cooper–Schrieffer to Bose–Einstein-condensate superfluids under artificial spin–orbit fields *Phys. Rev.* A **85** 033601

[55] Cheng M, Lutchyn R M, Galitski V and Das Sarma S 2009 Splitting of Majorana-fermion modes due to intervortex tunneling in a $p_x + ip_y$ superconductor *Phys. Rev. Lett.* **103** 107001

[56] Kraus Y E, Auerbach A, Fertig H A and Simon S H 2009 Majorana fermions of a two-dimensional $p_x + ip_y$ superconductor *Phys. Rev.* B **79** 134515

[57] Mizushima T and Machida K 2010 Splitting and oscillation of Majorana zero modes in the p-wave BCS-BEC evolution with plural vortices *Phys. Rev.* A **82** 023624

[58] Stewart J T, Gaebler J P and Jin D S 2008 Using photoemission spectroscopy to probe a strongly interacting Fermi gas *Nature* **454** 744–7

[59] Bakr W S, Gillen J I, Peng A, Fölling S and Greiner M 2009 A quantum gas microscope for detecting single atoms in a Hubbard-regime optical lattice *Nature* **462** 74–7

[60] Sherson J F, Weitenberg C, Endres M, Cheneau M, Bloch I and Kuhr S 2010 Single-atom-resolved fluorescence imaging of an atomic Mott insulator *Nature* **467** 68–72

[61] Dzuba V A and Flambaum V V 2010 Theoretical study of some experimentally relevant states of dysprosium *Phys. Rev.* A **81** 052515
[62] Dzuba V A, Flambaum V V and Lev B L 2011 Dynamic polarizabilities and magic wavelengths for dysprosium *Phys. Rev.* A **83** 032502
[63] Bermudez A, Amico L and Martin-Delgado M A 2010 Dynamical delocalization of Majorana edge states by sweeping across a quantum critical point *New J. Phys.* **12** 055014
[64] DeGottardi W, Sen D and Vishveshwara S 2011 Topological phases, Majorana modes and quench dynamics in a spin ladder system *New J. Phys.* **13** 065028
[65] Lu M, Burdick N Q, Youn S H and Lev B L 2011 Strongly dipolar Bose–Einstein condensate of dysprosium *Phys. Rev. Lett.* **107** 190401
[66] Lu M, Burdick N Q and Lev B L 2012 Quantum degenerate dipolar Fermi gas *Phys. Rev. Lett.* **108** 215301
[67] Aikawa K, Frisch A, Mark M, Baier S, Rietzler A, Grimm R and Ferlaino F 2012 Bose–Einstein condensation of erbium *Phys. Rev. Lett.* **108** 210401
[68] Pasquiou B, Bismut G, Beaufils Q, Crubellier A, Maréchal E, Pedri P, Vernac L, Gorceix O and Laburthe-Tolra B 2010 Control of dipolar relaxation in external fields *Phys. Rev.* A **81** 042716
[69] Fölling S, Trotzky S, Cheinet P, Feld M, Saers R, Widera A, Müller T and Bloch I 2007 Direct observation of second-order atom tunnelling *Nature* **448** 1029–32
[70] Tarruell L, Greif D, Uehlinger T, Jotzu G and Esslinger T 2012 Creating, moving and merging Dirac points with a Fermi gas in a tunable honeycomb lattice *Nature* **483** 302–5
[71] Akhmerov A R, Dahlhaus J P, Hassler F, Wimmer M and Beenakker C W J 2011 Quantized conductance at the Majorana phase transition in a disordered superconducting wire *Phys. Rev. Lett.* **106** 057001
[72] Brouwer P W, Duckheim M, Romito A and von Oppen F 2011 Topological superconducting phases in disordered quantum wires with strong spin–orbit coupling *Phys. Rev.* B **84** 144526
[73] Gangadharaiah S, Braunecker B, Simon P and Loss D 2011 Majorana edge states in interacting one-dimensional systems *Phys. Rev. Lett.* **107** 036801
[74] Stoudenmire E M, Alicea J, Starykh O A and Fisher M P A 2011 Interaction effects in topological superconducting wires supporting Majorana fermions *Phys. Rev.* B **84** 014503
[75] Sela E, Altland A and Rosch A 2011 Majorana fermions in strongly interacting helical liquids *Phys. Rev.* B **84** 085114
[76] Lutchyn R M and Fisher M P A 2011 Interacting topological phases in multiband nanowires *Phys. Rev.* B **84** 214528
[77] Kitaev A Y 2003 Fault-tolerant quantum computation by anyons *Ann. Phys.* **303** 2–30
[78] Freedman M H, Kitaev A, Larsen M J and Wang Z 2003 Topological quantum computation *Bull. Am. Math. Soc.* **40** 31–8
[79] Das Sarma S, Freedman M and Nayak C 2005 Topologically protected qubits from a possible non-Abelian fractional quantum Hall state *Phys. Rev. Lett.* **94** 166802
[80] Alicea J, Oreg Y, Refael G, Oppen F Von and Fisher M P A 2011 Non-Abelian statistics and topological quantum information processing in 1D wire networks *Nature Phys.* **7** 412–7
[81] Sarma S D, Nayak C and Tewari S 2006 Proposal to stabilize and detect half-quantum vortices in strontium ruthenate thin films: non-Abelian braiding statistics of vortices in a $p_x + \mathrm{ip_y}$ superconductor *Phys. Rev.* B **73** 220502